ACS OMEGA

http://pubs.acs.org/journal/acsodf

Article

Preparation of Acidic Electrolyzed Water by a RuO_2@TiO_2 Electrode with High Selectivity for Chlorine Evolution and Its Sterilization Effect

De Wang, Tianli Dong, Yaping Heng, Zhiqiang Xie, Hongwei Jiang, Miaojie Tian, Hucheng Jiang, Zhen Zhang, Zhandong Ren,* and Yuchan Zhu*

Cite This: *ACS Omega* 2022, 7, 23170−23178

Read Online

ACCESS | Metrics & More | Article Recommendations | Supporting Information

ABSTRACT: The food hygiene problems caused by bacterial biofilms in food processing equipment are directly related to human life safety and health. Therefore, it is of great strategic significance to study new food sterilization technology. An acidic electrolyzed water (AEW) disinfectant is an electrochemical sterilization technology which has the characteristics of wide adaptability, high efficiency, and environmental friendliness. However, since the sterilization efficiency of AEW for biofilms is not ideal, it is necessary to increase the available chlorine content (ACC) in AEW. A feasible method to increase the ACC is by increasing the chlorine evolution reaction (CER) selectivity of the electrode for AEW preparation. In this paper, the RuO_2@TiO_2 electrode was prepared by thermal decomposition combined with high-vacuum magnetron sputtering. Compared with the oxygen evolution reaction (OER) activity of an ordinary RuO_2 electrode, the OER activity of the RuO_2@TiO_2 electrode is significantly reduced. However, the CER activity of the RuO_2@TiO_2 electrode is close to the OER activity of RuO_2. The CER mechanism of the RuO_2@TiO_2 electrode is the second electron transfer, and the OER mechanism is the formation and transformation of OH_{ads}. The potential difference between the CER and OER of the RuO_2@TiO_2 electrode is 174 mV, which is 65 mV higher than that of the RuO_2 electrode, so the selectivity of the CER of the RuO_2@TiO_2 electrode is remarkably improved. During the preparation of AEW, the ACC obtained with the RuO_2@TiO_2 electrode is 1.7 times that obtained with the RuO_2 electrode. In the sterilization experiments on *Escherichia coli* and *Bacillus subtilis* biofilms, the logarithmic killing values of AEW prepared the by RuO_2@TiO_2 electrode are higher than those of AEW prepared by the RuO_2 electrode.

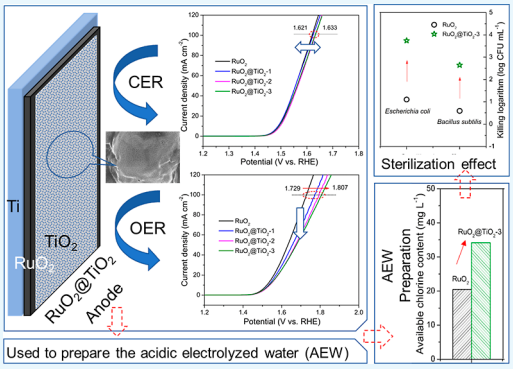

1. INTRODUCTION

Food-borne diseases are widespread in all parts of the world, especially the food hygiene problems caused by bacterial biofilms in food processing equipment. According to statistics, more than 80% of bacterial infections are related to bacterial biofilms in food processing equipment.[1−3] A bacterial biofilm is a complex microbial community with multiple cells, which has a three-dimensional self-assembled extracellular polymeric substance structure (extracellular polysaccharide, protein, extracellular DNA, etc.).[4−9] Compared with the planktonic cells, biofilms are more resistant to fungicides, so they are extremely difficult to kill.[10−12] Therefore, it is of great strategic significance to study new food sterilization technology with high efficiency, broad spectrum, safety, and no residue.

Electrochemical sterilization technology is a kind of nonthermal food sterilization technology, which is beneficial to maintain the physiological activity of functional components in food, as well as the color, aroma, taste, and nutritional components. The commonly used electrochemical sterilization technology is chemical sterilization by active chlorine (Cl_2, HOCl, and ClO^-) produced by electrolysis. An acidic electrolyzed water (AEW) disinfectant is an electrochemical sterilization technology which has been widely studied in recent years, and it has the characteristics of wide adaptability, high efficiency, and environmental friendliness.[13−21] At present, there are many research studies on the sterilization effect of AEW on the planktonic cells but few research studies on the bactericidal effect of the biofilms in food processing.[22−27] In addition, AEW can also be used in combination with other sterilization technologies for food sterilization, such as ultrasonic,[28] ultraviolet,[29] ozone,[30] fumaric acid,[31] ascorbic acid,[32] and antioxidants.[33]

AEW is generated by electrolysis of an extremely dilute NaCl solution. In order to improve the sterilization efficiency

Received: February 22, 2022
Accepted: June 16, 2022
Published: June 26, 2022

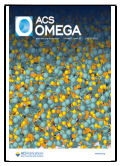

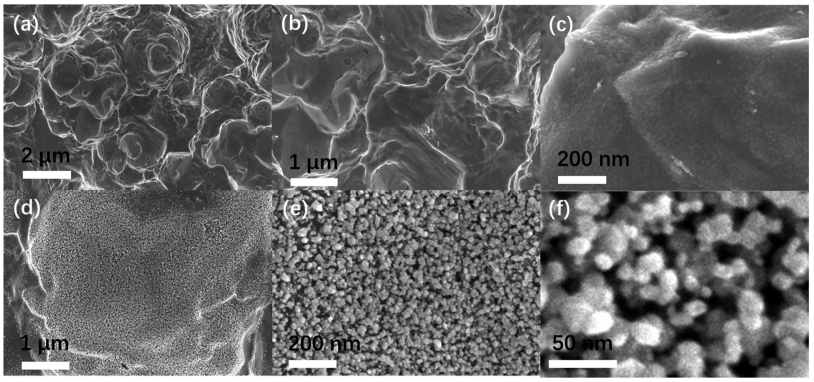

Figure 1. SEM images of RuO_2 (a–c) and RuO_2@TiO_2-3 (d–f) electrodes.

of AEW on biofilms, it is necessary to increase the content of available chlorine in AEW. In the process of electrolysis, accompanied by the occurrence of the chlorine evolution reaction (CER), the oxygen evolution side reaction (OER) is carried out simultaneously. Especially when the Cl^- content of the electrolyte used in the preparation of AEW is very low (0.1 g L^{-1}), the potential of chlorine evolution (E = 1.52 V) of the electrode material is very close to the potential of oxygen evolution ($E = E^0 + \eta$ = 1.29 V + 0.2 V = 1.49 V). If the concentration of NaCl decreases from 4 to 1 mol L^{-1}, the selectivity of the CER of the Ti–Ru–Ir electrode decreases from 90 to 80%.[34] In addition, different electrode materials possess different overpotentials for the CER and OER, which leads to different selectivities of the CER in the electrochemical reaction process.[35] Therefore, it is necessary to modify and optimize the electrode materials to improve the selectivity of the CER. In theoretical analysis, density functional theory (DFT) thermodynamic analysis can predict the activity of the CER and OER of the anode.[36−40] In 2014, the DFT calculation of a typical dimension-stable anode (DSA) of ruthenium–titanium oxide was studied by Karlsson et al.[37] Meanwhile, some new electrodes have been made in experiments, such as RuO_2–IrO_2–SnO_2–Sb_2O_5,[41] $Ru_{1-x}Mg_xO_2$,[42] $Ir_{1-x}Ni_xO_2$,[43] IrO_2–Ta_2O_5,[44] and IrO_2–Ta_2O_5–TiO_2.[45] In addition, the DFT calculation of the monolayers of TiO_2 on the RuO_2 (RuO_2@TiO_2) electrode have also been studied by Exner et al.[39] According to DFT calculations, using the RuO_2 electrode modified with 1 ML TiO_2 can reduce its CER and OER activities, but the OER activity decreases more notably, so the CER selectivity is improved (increased by several orders of magnitude). However, at present, there is little experimental research on the CER selectivity of the RuO_2@TiO_2 electrode.[46] Moreover, the highly CER-selective electrode aimed at increasing the available chlorine content (ACC) of AEW is also rarely investigated.[44,45]

In this paper, a RuO_2-coated electrode prepared by the thermal decomposition method was used as the substrate, and trace TiO_2 was modified on the surface of the RuO_2-coated electrode by the high-vacuum magnetron sputtering method. Then, the RuO_2@TiO_2 electrode was obtained. X-ray diffraction (XRD), scanning electron microscopy (SEM), and X-ray fluorescence (XRF) spectroscopy were used to characterize the crystal structure, surface morphology, and TiO_2 loading of the RuO_2@TiO_2 electrode. Furthermore, linear sweep voltammetry (LSV) was used to study the CER and OER activities of the RuO_2 electrode and RuO_2@TiO_2 electrode. The results indicate that the OER activity of the RuO_2@TiO_2 electrode is lower than that of the RuO_2 electrode, but the CER activity of the RuO_2@TiO_2 electrode is close to that of the RuO_2 electrode. Therefore, the CER selectivity of the RuO_2@TiO_2 electrode is much higher than that of the RuO_2 electrode. The preparation of AEW with the RuO_2@TiO_2 electrode can increase the content of available chlorine in AEW, and the generated ACC is 1.7 times that of the RuO_2 electrode, thus improving its sterilization efficiency on biofilms.

2. RESULTS AND DISCUSSION

The ultra-low loading of TiO_2 can be achieved by low-power magnetron sputtering. When the sputtering time is 120, 240, and 480 s, the TiO_2 loading of RuO_2@TiO_2-1 (120 s), RuO_2@TiO_2-2 (240 s), and RuO_2@TiO_2-3 (480 s) electrodes is 0.114, 0.124, and 0.155 μg cm^{-2}, respectively (Table S1). The surface morphology of RuO_2 and RuO_2@TiO_2 electrodes is characterized by SEM. SEM images of RuO_2 electrodes prepared by thermal decomposition are shown in Figure 1a–c. A relatively dense structure is formed on the surface of the RuO_2 electrode. The surface of the RuO_2 electrode is smooth, without prominent particles or cracks. Figure 1d–f shows the SEM images of the RuO_2@TiO_2-3 electrode. During magnetron sputtering, Ti atoms bombarded by Ar^+ react with O_2 molecules in the vacuum chamber to form TiO_2, which is deposited on the substrate in the form of molecular clusters. A layer of TiO_2 nanoparticles is uniformly deposited on the surface of the RuO_2 electrode, as shown in Figures 1d,e and S1. Moreover, the deposited TiO_2 particles are very small, with a size of about 10–20 nm, as shown in Figure 1f.

Figure 2 shows the XRD pattern of RuO_2 and RuO_2@TiO_2 electrodes. In the XRD pattern of RuO_2, many diffraction peaks can be observed, which belong to the characteristic diffraction peaks of RuO_2 and the Ti matrix. The diffraction peaks at 38.4, 40.2, 53.0, 63.0, 70.7, and 76.3° correspond to the (002), (101), (102), (110), (103), and (112) crystal planes of the Ti matrix, respectively, while the diffraction peak at 35.1° corresponds to the RuO_2(101) crystal plane. In Figure 2, it can be observed that the diffraction peak of the Ti matrix is due to the extremely thin surface layer of RuO_2 (the loading of RuO_2 is 60 μg cm^{-2}). Further observation indicates that there is no difference between the diffraction peak of the RuO_2@TiO_2 electrode and that of the RuO_2 electrode. Moreover, there is no difference in the characteristic diffraction peaks of RuO_2@TiO_2 electrodes with different TiO_2 loadings, as shown in Figure S2. No characteristic diffraction peak of TiO_2 is

https://doi.org/10.1021/acsomega.2c01077
ACS Omega 2022, 7, 23170−23178

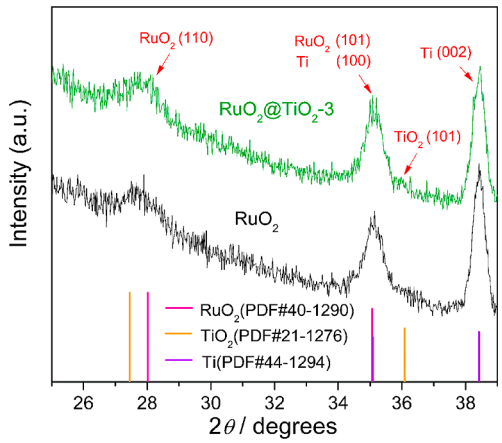

Figure 2. XRD patterns of RuO_2 and RuO_2@TiO_2-3 electrodes.

observed, which indicates that TiO_2 does not exist in a crystalline form. Of course, this is also related to the extremely low loading and very small particle size of TiO_2 deposited on the surface of the RuO_2 electrode by magnetron sputtering.

The electrochemical characteristics of the electrode can be analyzed by cyclic voltammetry (CV). In Figure S3, it can be seen that the electrochemical characteristics of RuO_2 and RuO_2@TiO_2 electrodes are basically the same. At a potential of 0.6 V, the redox peaks of Ru^{3+}/Ru^{4+} can be clearly observed for all electrodes. It is confirmed that the deposition of trace TiO_2 on the surface of the electrode does not change the original electrochemical characteristics of the RuO_2 electrode.

The electrochemical surface area (ECSA) represents the surface area that can actually participate in the electrochemical catalytic reaction. It can be obtained by analyzing the relationship between the current density (j) and scan rate (ν) of the double-layer capacitance region [0.38−0.48 V vs reversible hydrogen electrode (RHE)], as shown in Figure S4. According to Figure S4, the ECSAs of RuO_2 and RuO_2@TiO_2 electrodes are calculated and listed in Figure 3a. The ECSA of the RuO_2 electrode is 35 cm^2. After the addition of TiO_2, the ECSAs of RuO_2@TiO_2 electrodes increase significantly, reaching 58 (RuO_2@TiO_2-1), 55 (RuO_2@TiO_2-2), and 59 cm^2 (RuO_2@TiO_2-3). However, there is little difference in the ECSAs of RuO_2@TiO_2 electrodes with different TiO_2 loadings.

For the DSA electrode, the total surface charge (q_{tot}*) can be divided into the inner surface charge (q_{in}*) and outer surface charge (q_{out}*). It can be obtained by analyzing the relationship between q* and the scan rate (ν) of the CV curves (0−1.3 V vs RHE) given in Figure S5. As can be seen from Figure 3b, the q_{tot}* of the RuO_2 electrode is only 16.1 mC cm^{-2}. After the doping of TiO_2 on the surface of the RuO_2 electrode, the q_{tot}* of the RuO_2@TiO_2 electrode is increased to 21.3−23.3 mC cm^{-2}. By further observing the changes of q_{in}* and q_{out}* of different electrodes, the following conclusions can be obtained. For q_{in}*, there is no significant difference between the RuO_2 electrode and RuO_2@TiO_2 electrode. The q_{out}* of the RuO_2@TiO_2 electrode is significantly higher than that of the RuO_2 electrode. Therefore, it can be proven that the increase in q_{tot}* of the RuO_2@TiO_2 electrode comes from the increase in q_{out}*. The increase in q_{out}* may come from the deposition of TiO_2 in the process of magnetron sputtering.

The main bactericidal activity factor of AEW is the ACC, which is brought by the CER in the anode region. Therefore, it

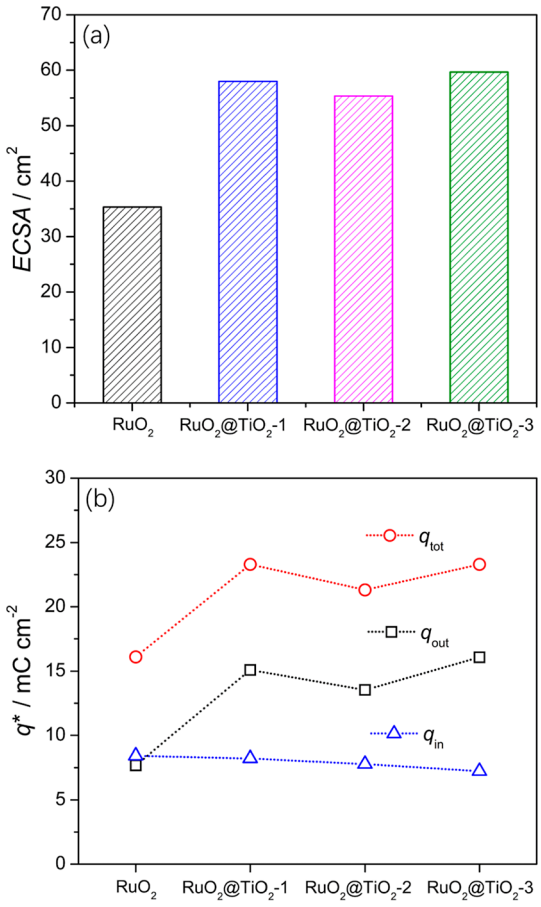

Figure 3. ECSA (a) and surface charges (b) of RuO_2 and RuO_2@TiO_2-1, -2, and -3 electrodes.

is very important to study the CER activity of different electrodes. The higher the activity of the CER is, the higher the ACC is. Considering the apparent activity of the CER, there is little difference between RuO_2 and RuO_2@TiO_2 electrodes, as shown in Figure 4a. The potential difference at a current density of 100 mA cm^{-2} is only 12 mV. If the different ECSA of all electrodes is further considered, the specific activity of the CER is obtained, as shown in Figure 4b. The specific activity of the CER of the RuO_2 electrode is higher than that of other RuO_2@TiO_2 electrodes. For the RuO_2 electrode, the potential with a specific activity of the CER of 1 mA cm^{-2} is 1.537 V. For the RuO_2@TiO_2 electrode-3 with the worst specific activity of the CER, its potential is 1.575 V. The difference between them is only 38 mV. It is mainly due to the fact that during the preparation of the RuO_2@TiO_2 electrode, the ECSA of the electrode is increased by depositing TiO_2 on the surface of the RuO_2 electrode. However, the addition of TiO_2 does not improve the apparent activity of the CER. Therefore, the CER specific activity of the RuO_2@TiO_2 electrode is a little worse than that of the RuO_2 electrode. For RuO_2@TiO_2 electrodes with different TiO_2 loadings, the difference of the specific activity of the CER is even smaller, only 7 mV. Therefore, the above results can prove that the addition of trace TiO_2 has some influence on the activity of the CER, but the influence is not significant.

The mechanism of the CER is further analyzed by Tafel curves shown in Figure 5. The Tafel slopes of RuO_2 and RuO_2@TiO_2 electrodes are both in the range of 41.9−46.9 mV dec^{-1}, which indicates that the CER mechanism should be the

https://doi.org/10.1021/acsomega.2c01077
ACS Omega 2022, 7, 23170−23178

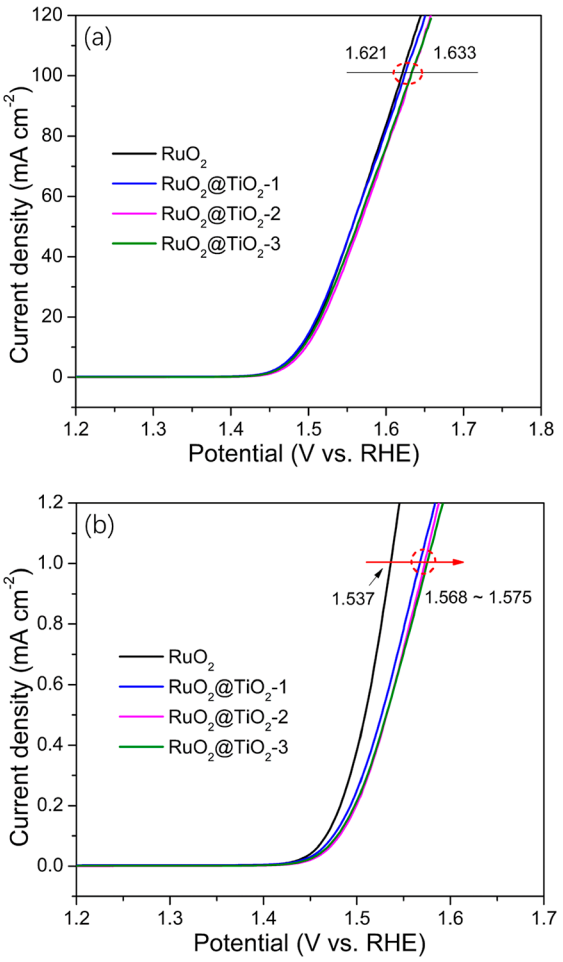

Figure 4. Apparent activity (a) and specific activity (b) of the CER of RuO_2 and RuO_2@TiO_2-1, -2, and -3 electrodes with the LSV curves in 4.0 M NaCl (pH = 1.0) at a sweeping rate of 5 mV s^{-1}.

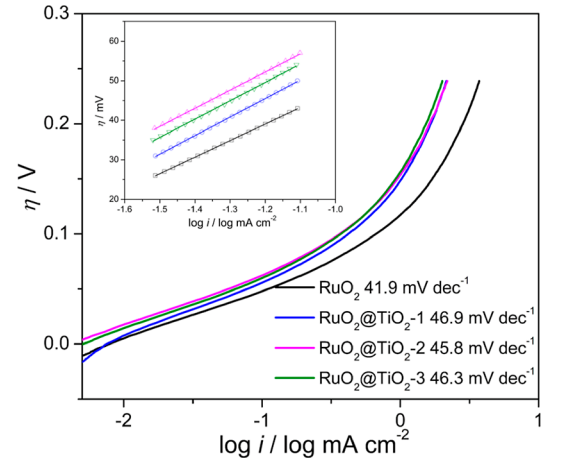

Figure 5. Tafel curves of the CER of RuO_2 and RuO_2@TiO_2-1, -2, and -3 electrodes.

unconventional electrochemical desorption scheme[47] (eqs 1−3). Here, step 2 (the second electron transfer) is a rate-limiting step; its Tafel slope is 40 mV dec^{-1}. Therefore, the rate-limiting step of the CER on the surface of the electrode should be an electron-transfer step and not an adsorption step. This can further explain why the apparent activity of the CER has nothing to do with the ECSA of the electrode.

$$S + Cl^- \rightarrow S - Cl + e \quad (1)$$

$$S - Cl \rightarrow S - Cl^+ + e \quad (2)$$

$$S - Cl^+ + Cl^- \rightarrow S + Cl_2 \quad (3)$$

In the preparation of AEW, the NaCl solution with a very low concentration is used as an electrolyte (C_{NaCl} < 0.1 wt %), so there is a large amount of OER in the anode region in addition to CER. Therefore, in order to improve the selectivity of the CER, it is necessary to reduce the activity of the OER. From the above results, it can be proven that the addition of TiO_2 has little effect on the apparent activity of the CER, which is consistent with Exner's theoretical calculation results.[36] At the same time, Exner's theoretical calculation has also indicated that the addition of TiO_2 has a great influence on the OER activity of the RuO_2 electrode. It will greatly reduce the OER activity and substantially improve the selectivity of the CER. Therefore, it is very important to study the OER activities of RuO_2@TiO_2 electrodes. In Figure 6a, it can be clearly seen that the apparent activity of the RuO_2 electrode is significantly higher than that of RuO_2@TiO_2 electrodes. Moreover, with an increase in TiO_2 loading, its apparent activity gradually decreases. When the current density

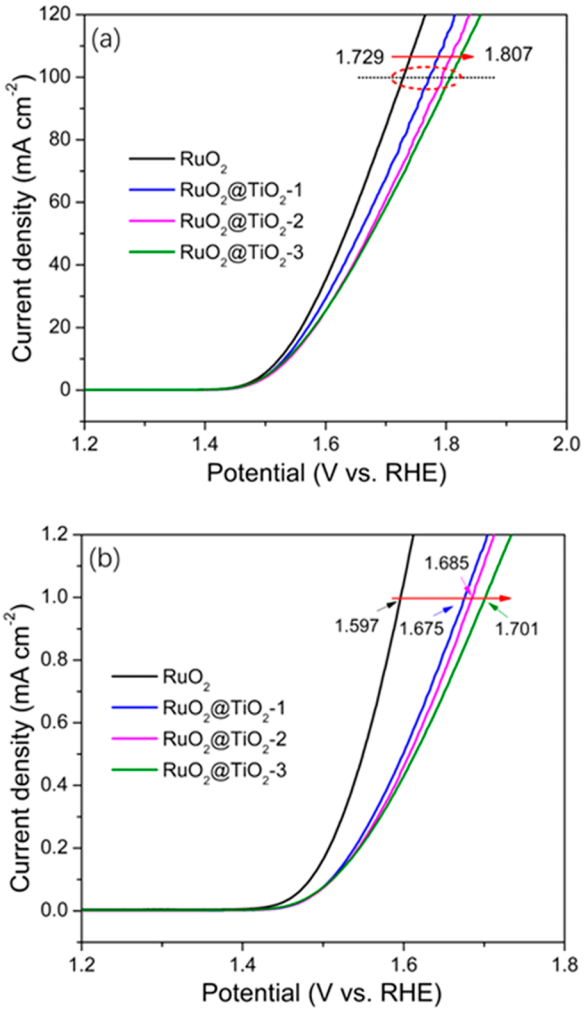

Figure 6. Apparent activity (a) and specific activity (b) of the OER of RuO_2 and RuO_2@TiO_2-1, -2, and -3 electrodes with the LSV curves in 0.5 M H_2SO_4 + 1.33 M Na_2SO_4 at a sweeping rate of 5 mV s^{-1}.

https://doi.org/10.1021/acsomega.2c01077
ACS Omega 2022, 7, 23170−23178

reaches 100 mA cm^{-2}, the potential of the RuO_2 electrode is 1.729 V. However, for the RuO_2@TiO_2 electrode, its potential is 1.771 (RuO_2@TiO_2-1), 1.793 (RuO_2@TiO_2-2), and 1.807 V (RuO_2@TiO_2-3), respectively. Compared with the potential of the RuO_2 electrode, the potential increases by 42 (RuO_2@TiO_2-1), 64 (RuO_2@TiO_2-2), and 78 mV (RuO_2@TiO_2-3), respectively. While for the CER, the potential difference between RuO_2 and RuO_2@TiO_2 electrodes is only 9 mV. Therefore, from an experimental point of view, it is proven for the first time that the addition of TiO_2 has a greater influence on the OER activity of the RuO_2 electrode than on the CER activity. If the influence of the ECSA on the apparent activity of the OER is further considered, the specific activity of the OER can be obtained, as shown in Figure 6b. When the specific activity is 1 mA cm^{-2}, the potential of the RuO_2 electrode is only 1.597 V. For the RuO_2@TiO_2 electrode, its potential is 1.675 (RuO_2@TiO_2-1), 1.685 (RuO_2@TiO_2-2), and 1.701 V (RuO_2@TiO_2-3), respectively. Compared with the potential of the RuO_2 electrode, the potential increases by 78 (RuO_2@TiO_2-1), 88 (RuO_2@TiO_2-2), and 104 mV (RuO_2@TiO_2-3), respectively. Obviously, the influence of TiO_2 addition on the specific activity of RuO_2@TiO_2 is more significant than that on the apparent activity. Therefore, the TiO_2 loading has a significant effect on OER activity, which is reflected in the fact that OER activity gradually decreases with an increase in TiO_2 loading.

Because the OER activity of the RuO_2@TiO_2 electrode decreased significantly, it is necessary to analyze the mechanism of the OER. In Figure 7, the Tafel analysis of

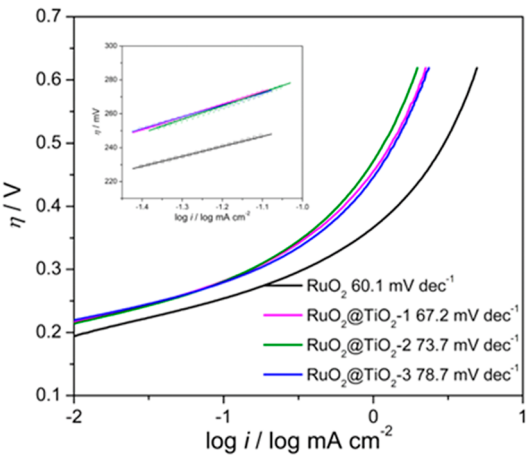

Figure 7. Tafel curves of the OER of the RuO_2 and RuO_2@TiO_2-1, -2, and -3 electrodes.

RuO_2@TiO_2 and RuO_2 electrodes is carried out. The Tafel slopes of RuO_2@TiO_2 electrodes are in the range of 67.2−78.7 mV dec^{-1}. However, the Tafel slope of RuO_2 is only 60.1 mV dec^{-1}. In the acid solution system, it is generally believed that the mechanism of the OER is as follows (eqs 4−8). If the symmetry factor β is 0.5, and eqs 4−6 are rate-limiting steps, respectively, the Tafel slopes are 120, 60, and 40 mV dec^{-1}, respectively. Therefore, the value of the Tafel slope of the RuO_2 electrode is near 60 mV dec^{-1}, indicating that the reaction-control step is the formation and transformation of OH_{ads}. As for the RuO_2@TiO_2 electrode, the increased Tafel slope indicates that the reaction rate of the rate-limiting step decreases. This is because the electronic properties of the RuO_2 electrode will change after adding TiO_2. In XPS spectra shown in Figure S6, the binding energy peak of the Ti^{4+} 2p orbital can be clearly observed, which proves the existence of TiO_2 on the electrode surface. In Figure S7, the binding energy peaks of the Ru^{4+}/Ru^{3+} $3p_{1/2}$ orbital of the RuO_2@TiO_2-3 electrode shift negatively by 0.1−0.2 eV compared with those of the RuO_2 electrode. The change in the electronic properties will lead to the weakening of the oxygen adsorption energy on the surface of the RuO_2@TiO_2-3 electrode, thus reducing the reaction rate in step 5. This is also consistent with Exner's calculation results.

$$S + H_2O \rightarrow S - OH^*_{ads} + H^+ + e \quad (4)$$

$$S - OH^*_{ads} \rightarrow S - OH_{ads} \quad (5)$$

$$S - OH_{ads} \rightarrow S - O_{ads} + H^+ + e \quad (6)$$

$$S - OH_{ads} + S - OH_{ads} \rightarrow S - O_{ads} + H_2O \quad (7)$$

$$S - O_{ads} + S - O_{ads} \rightarrow 2S + O_2 \quad (8)$$

As shown in Figures 4 and 6, the potential difference between the CER and OER ($\Delta E_{CER\text{-}OER}$) of the RuO_2 electrode is only 109 mV at a current density of 100 mA cm^{-2}. However, for the RuO_2@TiO_2-3 electrode, the $\Delta E_{CER\text{-}OER}$ is 174 mV, far exceeding that of the RuO_2 electrode. The $\Delta E_{CER\text{-}OER}$ of the RuO_2@TiO_2-3 electrode is significantly higher than that of the RuO_2 electrode, which indicates that the RuO_2@TiO_2-3 electrode has excellent CER selectivity. If the influence of ECSA is considered, $\Delta E_{CER\text{-}OER}$ is compared under the same specific activity. When the specific activity was 1.0 mA cm^{-2}, the $\Delta E_{CER\text{-}OER}$ of the RuO_2 electrode is 60 mV, while the $\Delta E_{CER\text{-}OER}$ of the RuO_2@TiO_2 electrode increases to 126 mV. At this time, the $\Delta E_{CER\text{-}OER}$ of the RuO_2@TiO_2-3 electrode is still significantly higher than that of the RuO_2 electrode. The large $\Delta E_{CER\text{-}OER}$ greatly inhibited the occurrence of the OER and enormously improved the selectivity of the CER. If the loading of TiO_2 is further increased greatly, the CER and OER activities of RuO_2@TiO_2 both decrease obviously, as shown in Figure S8. Further analysis of the CER stability of the RuO_2@TiO_2-3 electrode indicates that the CER activity has not changed significantly after the 13 h chronoamperometry experiment at a potential of 2.0 V, as shown in Figure S9.

Therefore, the RuO_2@TiO_2 electrode has excellent CER selectivity and is suitable for the preparation of AEW at a low concentration of NaCl. Then, the ACC analysis of AEW prepared by RuO_2 and RuO_2@TiO_2 electrodes is shown in Figure 8a. As far as the ACC is concerned, the ACC of AEW obtained by electrolysis with the RuO_2@TiO_2-3 electrode is 34.17 mg L^{-1}, which is 1.7 times that obtained by electrolysis with the RuO_2 electrode (20.46 mg L^{-1}). Moreover, the current efficiency of ACC in AEW prepared by the RuO_2@TiO_2-3 electrode is 25.83%, which is also obviously higher than that by the RuO_2 electrode, as shown in Figure S10. Thus, it can be proven that the electrolysis efficiency of the CER of the RuO_2@TiO_2 electrode is higher than that of the RuO_2 electrode, and it will generate the more ACC during the preparation of AEW.

Furthermore, AEW prepared by RuO_2 and RuO_2@TiO_2 electrodes was used for sterilization experiments. Bacterial biofilms of *Escherichia coli* and *Bacillus subtilis* were sterilized, and the killing logarithm values are shown in Figure 8b. The killing logarithm values of *E. coli* and *B. subtilis* of AEW

https://doi.org/10.1021/acsomega.2c01077
ACS Omega 2022, 7, 23170−23178

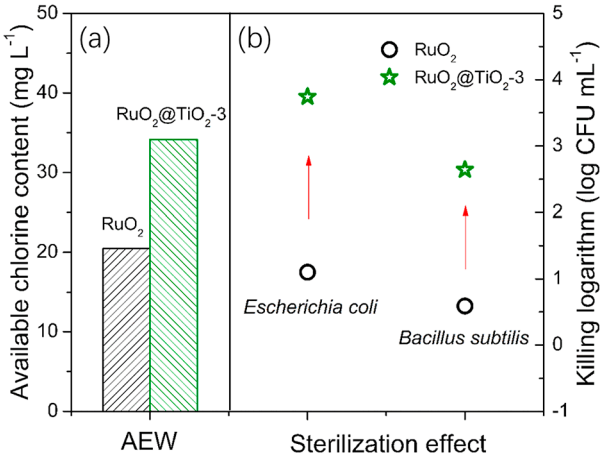

Figure 8. ACC in AEW prepared by the RuO_2 and RuO_2@TiO_2-3 electrodes (a). Logarithmic killing values of *E. coli* and *B. subtilis* of AEW prepared by the RuO_2 and RuO_2@TiO_2-3 electrodes (b).

prepared by the RuO_2 electrode are 1.1 and 0.59 $\log_{10}$ CFU/mL, respectively. The logarithmic killing values of AEW prepared by the RuO_2@TiO_2 electrode of *E. coli* and *B. subtilis* are 3.74 and 2.64 $\log_{10}$ CFU/mL, respectively. Obviously, the sterilization effect of AEW prepared by the RuO_2@TiO_2 electrode is good because the ACC of AEW prepared by the RuO_2@TiO_2 electrode is high. The high ACC of AEW is due to the high CER selectivity of the RuO_2@TiO_2 electrode. In this way, through the regulation of electrode materials, the CER selectivity of the electrode is changed, and AEW is prepared more efficiently, thus obtaining more efficient sterilization efficiency.

3. CONCLUSIONS

In order to enhance the ACC in AEW and thesterilization efficiency of biofilms, it is necessary to improve the CER selectivity of the electrode for AEW preparation. In this paper, the RuO_2@TiO_2 electrode was prepared by thermal decomposition combined with high-vacuum magnetron sputtering. Compared with the OER activity of an ordinary RuO_2 electrode, the OER activity of the RuO_2@TiO_2 electrode is greatly reduced. However, the CER activity of the RuO_2@TiO_2 electrode is close to the OER activity of RuO_2. The potential difference between the CER and OER of the RuO_2@TiO_2 electrode is 175 mV, which is 58 mV higher than that of the RuO_2 electrode, thus improving the selectivity of the CER of the RuO_2@TiO_2 electrode. The CER mechanism of the RuO_2@TiO_2 electrode is the second electron transfer, and the OER mechanism is the formation and transformation of OH_{ads}. The RuO_2@TiO_2 electrode was used in AEW preparation, and the ACC produced by it was 1.7 times that produced by the RuO_2 electrode. The logarithmic killing values of both *E. coli* and *B. subtilis* biofilms of AEW prepared by the RuO_2@TiO_2 electrode are higher than those of AEW prepared by the RuO_2 electrode.

4. EXPERIMENTAL METHODS

4.1. Electrode Preparation. A Ti plate was utilized as the electrode substrate, which was sand-blasted and degreased in 2 mol L^{-1} H_2SO_4 with ultrasonication. Then, a gray surface with a uniform roughness was produced by boiling it in 10 wt % $H_2C_2O_4$ at 96 °C for 1 h. The preparation of the RuO_2 electrode by thermal decomposition is described in detail as follows. The $RuCl_3{\cdot}3H_2O$ precursors were dissolved in the 1:1 volume ratio ethanol and n-butanol mixed solutions. The ion concentration of Ru^{3+} was 0.02 mol L^{-1}. After the solution was uniformly dispersed by ultrasonication, 30 μL of the solution was dripped onto the Ti foil. When the surface solvent was completely volatilized, it was calcined at 400 °C in a muffle furnace for 1 h. The Ru loading was about 60 $\mu g\ cm^{-2}$. The RuO_2 electrode processed above was placed on the sample stage of the vacuum chamber of the high-vacuum magnetron sputtering apparatus (TRP-450, SKY Technology Development Co., Ltd). During the experiment, a Ti target with a purity of 99.99% was used as a sputtering target and connected to a DC power supply. The vacuum chamber was evacuated to 4×10^{-4} Pa before sputtering. Then, a mixture gas of Ar and O_2 was introduced, and their flow rates were 20 and 10 mL min^{-1}, respectively. The pressure of the vacuum chamber was adjusted to 1.0−1.2 Pa. When the sputtering time was 120, 240, and 480 s, respectively, the obtained samples were recorded as RuO_2@TiO_2-1, RuO_2@TiO_2-2, and RuO_2@TiO_2-3 electrodes.

4.2. Material Characterization. SEM images were captured with a Zeiss SIGMA field-emission scanning electron microscope. XRD patterns were acquired using an XRD-7000 X-ray diffractometer. Analysis of the composition of the electrode was carried out by XRF (EDX-7000, Shimadzu, Japan).

4.3. Electrochemical Measurements. In the electrochemical experiment, a three-electrode system was used for testing using the CHI600E instrument. The working electrodes are RuO_2 and RuO_2@TiO_2 electrodes. The counter electrode and the reference electrode are a platinum wire and the $Hg_2SO_4/Hg/K_2SO_4$ (0.1 mol L^{-1}) electrode, respectively. CV was carried out in the potential range of 0−1.3 V vs RHE in a 0.5 mol L^{-1} H_2SO_4 solution. The double-layer capacitance scanning was performed in the potential range of 0.38−0.48 V vs RHE in a 0.5 mol L^{-1} H_2SO_4 solution. The CER activity was characterized by LSV in a 4.0 mol L^{-1} (pH = 1) NaCl solution at a scanning speed of 5 mV s^{-1} in the range of 1.2−1.7 V. The OER activity was characterized by LSV in a 0.5 mol L^{-1} H_2SO_4 + 1.33 mol L^{-1} Na_2SO_4 solution at a scanning speed of 5 mV s^{-1} in the range of 1.2−1.9 V.

4.4. AEW Preparation and Analysis. 0.1 wt % NaCl was electrolyzed to produce AEW in an anion-exchange membrane electrolytic cell with a volume of 50 mL. The anode was the RuO_2 or RuO_2@TiO_2-3 electrode and the cathode was a Ti plate. The electrode area was 1 cm^2. The current density was 20 mA cm^{-2}, and the electrolysis time was 30 min. The concentration of total active chlorine dissolved in the solution was determined using the 3,3′,5,5′-tetramethylbenzidine (TMB) colorimetric method. In this method, TMB was oxidized to form a yellow product, and its concentration was analyzed immediately using a spectrophotometer (TU-1900, Beijing Purkinje General Instrument Co., Ltd.) at 450 nm.

4.5. Sterilization Effect of AEW. *E. coli* (ATCC8739, purchased from Guangdong Huankai Microbial Sci. & Tech. Co., Ltd) and *B. subtilis* (ATCC9372, purchased from Guangdong Huankai Microbial Sci. & Tech. Co., Ltd) were used as representatives of Gram-negative and Gram-positive bacteria, respectively. The bacterial culture solutions were grown at 37 °C for 24 h, and the final concentration reached about 10^8 CFU mL^{-1}. The biofilm carrier is a stainless steel sheet, which was cut into a 1 × 1 cm square sheet. First, the stainless steel sheet was soaked in absolute ethyl alcohol

https://doi.org/10.1021/acsomega.2c01077
ACS Omega 2022, 7, 23170−23178

overnight to remove the grease on the surface, and then, it was cleaned by ultrasonication with 5 mol L^{-1} hydrochloric acid for 15 min, and finally, it was rinsed with distilled water 3−5 times. The treated stainless steel plate was put into a test tube containing 10 mL of the nutrient agar medium, and then, 0.1 mL of the above bacterial suspension was added. The bacterial biofilm was obtained by continuous culture for 7 days (changing the culture solution every 24 h) in a constant temperature oscillator at 37 °C and 150 rpm. The cultured biofilm was taken out and washed with phosphate-buffered saline solution. The biofilm was placed into the test tube containing 10 mL of AEW for sterilization for 10 s and then quickly moved to the test tube containing 10 mL of the sodium thiosulfate neutralizer to stop sterilization. The biofilm was removed after sterilization, to which 10 mL of normal saline was added, and then, it was peeled off by ultrasonication for 15 min (100 W, 25 °C). The survival of *E. coli* or *B. subtilis* was determined by the colony counting method using a nutrient agar plate.

■ ASSOCIATED CONTENT

Supporting Information

The Supporting Information is available free of charge at https://pubs.acs.org/doi/10.1021/acsomega.2c01077.

SEM mapping of the RuO_2@TiO_2-3 electrode; XRD patterns of RuO_2 and RuO_2@TiO_2-1, -2, and -3 electrodes; cyclic voltammograms of RuO_2 and RuO_2@TiO_2-1, -2, and -3 electrodes; cyclic voltammograms of RuO_2 and RuO_2@TiO_2-1, -2, and -3 electrodes with different scan rates at a potential of 0.38−0.48 V; double-layer capacitances of RuO_2 and RuO_2@TiO_2-1, -2, and -3; total surface charge (q_{tot}*) and outer surface charge (q_{out}*) of RuO_2 and RuO_2@TiO_2-1, -2, and -3) electrodes; XPS spectra of Ti 2p in the RuO_2@TiO_2-3 electrode, XPS spectra of Ru 3p in the RuO_2@TiO_2-3 and RuO_2 electrodes, CER and OER activities of RuO_2 and RuO_2@TiO_2-4 electrodes, chronoamperometry experimental results of the RuO_2@TiO_2-3 electrode at a potential of 2.0 V, current efficiencies of the ACC in AEW prepared by the RuO_2 and RuO_2@TiO_2-3 electrodes, and loading of TiO_2 of the RuO_2@TiO_2-1, -2, and -3 electrodes found by XRF (PDF)

■ AUTHOR INFORMATION

Corresponding Authors

Zhandong Ren − *School of Chemical and Environmental Engineering, Wuhan Polytechnic University, Wuhan 430023, P. R. China*; orcid.org/0000-0003-2249-9490; Phone: +86-27-83943956; Email: renzhandong@163.com

Yuchan Zhu − *School of Chemical and Environmental Engineering, Wuhan Polytechnic University, Wuhan 430023, P. R. China*; orcid.org/0000-0001-9935-5255; Phone: +86-27-83943956; Email: zhuyuchan@163.com

Authors

De Wang − *School of Chemical and Environmental Engineering, Wuhan Polytechnic University, Wuhan 430023, P. R. China*

Tianli Dong − *School of Chemical and Environmental Engineering, Wuhan Polytechnic University, Wuhan 430023, P. R. China*

Yaping Heng − *School of Chemical and Environmental Engineering, Wuhan Polytechnic University, Wuhan 430023, P. R. China*

Zhiqiang Xie − *School of Chemical and Environmental Engineering, Wuhan Polytechnic University, Wuhan 430023, P. R. China*

Hongwei Jiang − *School of Chemical and Environmental Engineering, Wuhan Polytechnic University, Wuhan 430023, P. R. China*

Miaojie Tian − *School of Chemical and Environmental Engineering, Wuhan Polytechnic University, Wuhan 430023, P. R. China*

Hucheng Jiang − *School of Chemical and Environmental Engineering, Wuhan Polytechnic University, Wuhan 430023, P. R. China*

Zhen Zhang − *School of Chemical and Environmental Engineering, Wuhan Polytechnic University, Wuhan 430023, P. R. China*

Complete contact information is available at: https://pubs.acs.org/10.1021/acsomega.2c01077

Notes

The authors declare no competing financial interest.

■ ACKNOWLEDGMENTS

The authors acknowledge financial support from the Natural Science Foundation of Hubei Province (grant no. 2020CFB777).

■ REFERENCES

(1) Yuan, L.; Hansen, M. F.; Røder, H. L.; Wang, N.; Burmølle, M.; He, G. Mixed-species biofilms in the food industry: Current knowledge and novel control strategies. *Crit. Rev. Food Sci. Nutr.* **2020**, *60*, 2277−2293.

(2) Zhu, Y.; Li, C.; Cui, H.; Lin, L. Feasibility of cold plasma for the control of biofilms in food industry. *Trends Food Sci. Technol.* **2020**, *99*, 142−151.

(3) Byun, K.-H.; Na, K. W.; Ashrafudoulla, M.; Choi, M. W.; Han, S. H.; Kang, I.; Park, S. H.; Ha, S.-D. Combination treatment of peroxyacetic acid or lactic acid with UV-C to control Salmonella Enteritidis biofilms on food contact surface and chicken skin. *Food Microbiol.* **2022**, *102*, 103906.

(4) Weerarathne, P.; Payne, J.; Saha, J.; Kountoupis, T.; Jadeja, R.; Jaroni, D. Evaluating the Efficacy of Sodium Acid Sulfate to Reduce Escherichia coli O157:H7 and its Biofilms on Food-Contact Surfaces. *LWT-Food Sci. Technol.* **2021**, *139*, 110501.

(5) Kim, M.-J.; Kim, J.-S. Enhanced inactivation of Salmonella enterica Enteritidis biofilms on the stainless steel surface by proteinase K in the combination with chlorine. *Food Control* **2022**, *132*, 108519.

(6) Shivaprasad, D.; Taneja, N. K.; Lakra, A.; Sachdev, D. In vitro and in situ abrogation of biofilm formation in E. coli by vitamin C through ROS generation, disruption of quorum sensing and exopolysaccharide production. *Food Chem.* **2021**, *341*, 128171.

(7) Zhang, Y.; Shigemura, K.; Duc, H. M.; Shen, C.; Huang, H.-H.; Sato, J.; Masuda, Y.; Honjoh, K.; Miyamoto, T. Effects of bacteriophage on inhibition and removal of mixed biofilm of enterohemorrhagic Escherichia coli O157:H7 and O91:H-. *LWT-Food Sci. Technol.* **2020**, *134*, 109945.

(8) Medina-Rodríguez, A. C.; Ávila-Sierra, A.; Ariza, J. J.; Guillamón, E.; Baños-Arjona, A.; Vicaria, J. M.; Jurado, E. Clean-in-place disinfection of dual-species biofilm (Listeria and Pseudomonas) by a green antibacterial product made from citrus extract. *Food Control* **2020**, *118*, 107422.

(9) Mazaheri, T.; Ripolles-Avila, C.; Hascoët, A. S.; Rodríguez-Jerez, J. J. Effect of an enzymatic treatment on the removal of mature

Listeria monocytogenes biofilms: A quantitative and qualitative study. *Food Control* **2020**, *114*, 107266.
(10) Yuan, L.; Sadiq, F. A.; Wang, N.; Yang, Z.; He, G. Recent advances in understanding the control of disinfectant-resistant biofilms by hurdle technology in the food industry. *Crit. Rev. Food Sci.* **2021**, *61*, 3876−3891.
(11) Byun, K.-H.; Han, S. H.; Yoon, J.-W.; Park, S. H.; Ha, S.-D. Efficacy of chlorine-based disinfectants (sodium hypochlorite and chlorine dioxide) on Salmonella Enteritidis planktonic cells, biofilms on food contact surfaces and chicken skin. *Food Control* **2021**, *123*, 107838.
(12) Hua, Z.; Younce, F.; Tang, J.; Ryu, D.; Rasco, B.; Hanrahan, I.; Zhu, M.-J. Efficacy of saturated steam against Listeria innocua biofilm on common food-contact surfaces. *Food Control* **2021**, *125*, 107988.
(13) Sun, J.; Jiang, X.; Chen, Y.; Lin, M.; Tang, J.; Lin, Q.; Fang, L.; Li, M.; Hung, Y.-C.; Lin, H. Recent trends and applications of electrolyzed oxidizing water in fresh foodstuff preservation and safety control. *Food Chem.* **2022**, *369*, 130873.
(14) Rahman, S.; Khan, I.; Oh, D.-H. Electrolyzed Water as a Novel Sanitizer in the Food Industry: Current Trends and Future Perspectives. *Compr. Rev. Food Sci. Food Saf.* **2016**, *15*, 471−490.
(15) Iram, A.; Wang, X.; Demirci, A. Electrolyzed Oxidizing Water and Its Applications as Sanitation and Cleaning Agent. *Food Eng. Rev.* **2021**, *13*, 411−427.
(16) Zhang, W.; Cao, J.; Jiang, W. Application of electrolyzed water in postharvest fruits and vegetables storage: A review. *Trends Food Sci. Technol.* **2021**, *114*, 599−607.
(17) Ampiaw, R. E.; Yaqub, M.; Lee, W. Electrolyzed water as a disinfectant: A systematic review of factors affecting the production and efficiency of hypochlorous acid. *J. Water Proc. Eng.* **2021**, *43*, 102228.
(18) Meireles, A.; Giaouris, E.; Simões, M. Alternative disinfection methods to chlorine for use in the fresh-cut industry. *Food Res. Int.* **2016**, *82*, 71−85.
(19) Li, X.; Farid, M. A review on recent development in non-conventional food sterilization technologies. *J. Food Eng.* **2016**, *182*, 33−45.
(20) Huang, Y.-R.; Hung, Y.-C.; Hsu, S.-Y.; Huang, Y.-W.; Hwang, D.-F. Application of electrolyzed water in the food industry. *Food Control* **2008**, *19*, 329−345.
(21) Al-Haq, M. I.; Sugiyama, J.; Isobe, S. Applications of electrolyzed water in agriculture & food industries. *Food Sci. Technol. Res.* **2005**, *11*, 135−150.
(22) Yan, J.; Xie, J. Removal of Shewanella putrefaciens Biofilm by acidic electrolyzed water on food contact surfaces. *LWT-Food Sci. Technol.* **2021**, *151*, 112044.
(23) Cai, L.-l.; Hu, H.-j.; Lu, Q.; Wang, H.-h.; Xu, X.-l.; Zhou, G.-h.; Kang, Z.-l.; Ma, H.-j. Morphophysiological responses of detached and adhered biofilms of Pseudomonas fluorescens to acidic electrolyzed water. *Food Microbiol.* **2019**, *82*, 89−98.
(24) Hu, H.; Cai, L.; Dong, Y.; Wang, H.; Xu, X.; Zhou, G. Modeling the degradation of acidic electrolyzed water and its disinfection of dual-species biofilm. *LWT-Food Sci. Technol.* **2019**, *104*, 159−164.
(25) Li, Y.; Tan, L.; Guo, L.; Zhang, P.; Malakar, P. K.; Ahmed, F.; Liu, H.; Wang, J. J.; Zhao, Y. Acidic electrolyzed water more effectively breaks down mature Vibrio parahaemolyticus biofilm than DNase I. *Food Control* **2020**, *117*, 107312.
(26) Roy, P. K.; Mizan, M. F. R.; Hossain, M. I.; Han, N.; Nahar, S.; Ashrafudoulla, M.; Toushik, S. H.; Shim, W.-B.; Kim, Y.-M.; Ha, S.-D. Elimination of Vibrio parahaemolyticus biofilms on crab and shrimp surfaces using ultraviolet C irradiation coupled with sodium hypochlorite and slightly acidic electrolyzed water. *Food Control* **2021**, *128*, 108179.
(27) Song, Y. J.; Yu, H. H.; Kim, Y. J.; Lee, N.-K.; Paik, H.-D. The use of papain for the removal of biofilms formed by pathogenic Staphylococcus aureus and Campylobacter jejuni. *LWT-Food Sci. Technol.* **2020**, *127*, 109383.
(28) Shao, L.; Dong, Y.; Chen, X.; Xu, X.; Wang, H. Modeling the elimination of mature biofilms formed by Staphylococcus aureus and Salmonella spp. Using combined ultrasound and disinfectants. *Ultrason. Sonochem.* **2020**, *69*, 105269.
(29) Jiang, Y.; Ai, C.; Liao, X.; Liu, D.; Ding, T. Effect of slightly acidic electrolyzed water (SAEW) and ultraviolet light illumination pretreatment on microflora inactivation of coriander. *LWT-Food Sci. Technol.* **2020**, *132*, 109898.
(30) Mohammad, Z.; Kalbasi-Ashtari, A.; Riskowski, G.; Juneja, V.; Castillo, A. Inactivation of Salmonella and Shiga toxin-producing Escherichia coli (STEC) from the surface of alfalfa seeds and sprouts by combined antimicrobial treatments using ozone and electrolyzed water. *Food Res. Int.* **2020**, *136*, 109488.
(31) Ngnitcho, P.-F. K.; Tango, C. N.; Khan, I.; Daliri, E. B. M.; Chellian, R.; Oh, D. H. The applicability of Weibull model for the kinetics inactivation of Listeria monocytogenes and Escherichia coli O157:H7 on soybean sprouts submitted to chemical sanitizers in combination with ultrasound at mild temperatures. *LWT-Food Sci. Technol.* **2018**, *91*, 573−579.
(32) Yan, W.; Zhang, Y.; Yang, R.; Zhao, W. Combined effect of slightly acidic electrolyzed water and ascorbic acid to improve quality of whole chilled freshwater prawn (Macrobrachium rosenbergii). *Food Control* **2020**, *108*, 106820.
(33) Saravanakumar, K.; Sathiyaseelan, A.; Mariadoss, A. V. A.; Chelliah, R.; Shin, S.; Park, S.; Oh, D.-H.; Wang, M.-H. Slightly acidic electrolyzed water combination with antioxidants and fumaric acid treatment to maintain the quality of fresh-cut bell peppers. *LWT-Food Sci. Technol.* **2021**, *147*, 111565.
(34) Zeradjanin, A. R.; Menzel, N.; Schuhmann, W.; Strasser, P. On the faradaic selectivity and the role of surface inhomogeneity during the chlorine evolution reaction on ternary Ti−Ru−Ir mixed metal oxide electrocatalysts. *Phys. Chem. Chem. Phys.* **2014**, *16*, 13741−13747.
(35) Ming, R.; Zhu, Y.; Deng, L.; Zhang, A.; Wang, J.; Han, Y.; Chai, B.; Ren, Z. Effect of electrode material and electrolysis process on the preparation of electrolyzed oxidizing water. *New J. Chem.* **2018**, *42*, 12143−12151.
(36) Exner, K. S.; Anton, J.; Jacob, T.; Over, H. Controlling selectivity in the chlorine evolution reaction over RuO_2-based catalysts. *Angew. Chem., Int. Ed.* **2014**, *53*, 11032−11035.
(37) Karlsson, R. K. B.; Hansen, H. A.; Bligaard, T.; Cornell, A.; Pettersson, L. G. M. Ti atoms in $Ru_{0.3}Ti_{0.7}O_2$ mixed oxides form active and selective sites for electrochemical chlorine evolution. *Electrochim. Acta* **2014**, *146*, 733−740.
(38) Karlsson, R. K. B.; Cornell, A.; Pettersson, L. G. M. The electrocatalytic properties of doped TiO_2. *Electrochim. Acta* **2015**, *180*, 514−527.
(39) Exner, K. S.; Anton, J.; Jacob, T.; Over, H. Full kinetics from first principles of the chlorine evolution reaction over a RuO_2(110) model electrode. *Angew. Chem., Int. Ed.* **2016**, *55*, 7501−7504.
(40) Hansen, H. A.; Man, I. C.; Studt, F.; Abild-Pedersen, F.; Bligaard, T.; Rossmeisl, J. Electrochemical chlorine evolution at rutile oxide (110) surfaces. *Phys. Chem. Chem. Phys.* **2010**, *12*, 283−290.
(41) Xiong, K.; Deng, Z.; Li, L.; Chen, S.; Xia, M.; Zhang, L.; Qi, X.; Ding, W.; Tan, S.; Wei, Z. Sn and Sb co-doped RuTi oxides supported on TiO_2 nanotubes anode for selectivity toward electrocatalytic chlorine evolution. *J. Appl. Electrochem.* **2013**, *43*, 847−854.
(42) Abbott, D. F.; Petrykin, V.; Okube, M.; Bastl, Z.; Mukerjee, S.; Krtil, P. Selective Chlorine Evolution Catalysts Based on Mg-Doped Nanoparticulate Ruthenium Dioxide. *J. Electrochem. Soc.* **2015**, *162*, H23−H31.
(43) Kuznetsova, E.; Petrykin, V.; Sunde, S.; Krtil, P. Selectivity of Nanocrystalline IrO_2-Based Catalysts in Parallel Chlorine and Oxygen Evolution. *Electrocatalysis* **2015**, *6*, 198−210.
(44) Ren, Z.; Quan, S.; Gao, J.; Li, W.; Zhu, Y.; Liu, Y.; Chai, B.; Wang, Y. The electrocatalytic activity of IrO_2−Ta_2O_5 anode materials and electrolyzed oxidizing water preparation and sterilization effect. *RSC Adv.* **2015**, *5*, 8778−8786.

https://doi.org/10.1021/acsomega.2c01077
ACS Omega 2022, 7, 23170−23178

(45) Deng, L.; Liu, Y.; Zhao, G.; Chen, J.; He, S.; Zhu, Y.; Chai, B.; Ren, Z. Preparation of electrolyzed oxidizing water by TiO_2 doped IrO_2-Ta_2O_5 electrode with high selectivity and stability for chlorine evolution. *J. Electroanal. Chem.* **2019**, *832*, 459−466.
(46) Finke, C. E.; Omelchenko, S. T.; Jasper, J. T.; Lichterman, M. F.; Read, C. G.; Lewis, N. S.; Hoffmann, M. R. Enhancing the activity of oxygen-evolution and chlorine-evolution electrocatalysts by atomic layer deposition of TiO_2. *Energy Environ. Sci.* **2019**, *12*, 358−365.
(47) Santana, M. H. P.; De Faria, L. A. Oxygen and chlorine evolution on RuO_2+TiO_2+CeO_2+Nb_2O_5 mixed oxide electrodes. *Electrochim. Acta* **2006**, *51*, 3578−3585.

https://doi.org/10.1021/acsomega.2c01077
ACS Omega 2022, 7, 23170−23178